A Novel Companding Technique to Reduce High Peak to Average Power Ratio in OFDM Systems

ABDULWAHID MOHAMMED[1], TAWFIK ISMAIL[2,3], (Senior Member, IEEE), AMIN NASSAR[1], AND HASSAN MOSTAFA[1,4], (Senior Member, IEEE)

[1]Department of Electronics and Communication Engineering, Cairo University, Giza 12613, Egypt
[2]National Institute of Laser Enhanced Sciences, Cairo University, Giza 12613, Egypt
[3]Wireless Intelligent Networks Center, Nile University, Giza 12677, Egypt
[4]University of Science and Technology, Zewail City of Science and Technology, Giza 12578, Egypt

Corresponding authors: Tawfik Ismail (tismail@cu.edu.eg) and Hassan Mostafa (hmostafa@zewailcity.edu.eg)

ABSTRACT The reduction of the high peak-to-average-power ratio (PAPR) is important to the efficiency of the orthogonal frequency division multiplexing (OFDM) technique. Excessive PAPR contributes to non-linear clipping induced harmonic distortions that reduce system reliability. In this article, a new technique for decreasing the high PAPR in OFDM with minimum effects on the system performance is proposed. The technique uses the image adjust (IMADJS) function to reduce the high PAPR of transmitted OFDM signals by compressing large signals and expanding small signals. In comparison, the IMADJS strategy has the advantage of maintaining a constant average power level before and after companding. A comparative analysis is provided between the proposed (IMADJS) technique and well-known companding techniques such as $\mu-$law, absolute exponential (AEXP), and the new error function (NERF). The comparison is based on PAPR, bit error rate (BER), power spectral density (PSD), and average power performance metrics. Simulation results confirm that the IMADJS technique significantly improved the drawbacks of the PAPR. Furthermore, the PAPR is reduced by 2.81dB. The IMADJS technique has less impact on the original power spectrum than on other companding schemes. The average out-of-band radiation of the IMADJS technique reaches about -50dB at the frequency of 0MHz. In contrast, the average of the original OFDM signal is that the out-of-band radiation reaches around -52dB. The AEXP and NERF companding techniques reach about -46dB, while the μ-law companding technique hits about -37dB.

INDEX TERMS Orthogonal frequency division multiplexing (OFDM), peak-to-average-power-ratio (PAPR), companding techniques, image adjustment (IMADJS) and performance evaluation.

I. INTRODUCTION

Orthogonal Frequency Division Multiplexing (OFDM) is a multi-carrier technique, which is effective and efficient in 4G and 5G mobile networks [1]–[3]. The OFDM divides the available bandwidth into several sub-bandwidths, whereas the data with low rates streams are parallel modulated simultaneously and carried over the sub-bandwidths. Due to this parallel transmission, the symbol duration increases, thus decrease the prorated amount of dispersion in time resulting from the multi-path delay spread. OFDM has several advantages that make it widely used for many communication

The associate editor coordinating the review of this manuscript and approving it for publication was Prakasam Periasamy.

systems [4]–[6]. The OFDM limits the propagation effects of multipath propagation, the impulses noise, and eliminates the need for equalizers. It uses modern digital signal processing techniques, such as the fast Fourier transform (FFT) technique. However, OFDM has the major drawback of having a large Peak-to-Average Power Ratio (PAPR). The large PAPR appears as a consequence of the multicarrier OFDM signal nature [7]. The OFDM signal, consisting of N individual and independent data symbols, when the N signals add up to the same phase, a substantial increase in the PAPR is observed. The observed instantaneous PAPR might reach as high values as N times of the average OFDM symbol amplitude [6]. In this case, high power amplifier (HPA) and digital to analog converter (DAC) are required to overcome the large dynamic

ranges and to avoid clipping the observed large amplitude of the OFDM symbol. On the other hand, adapting the dynamic range of the HPA and the DAC to the high PAPR values increases the power consumption and the implementation complexity of the transceiver design. Therefore, the PAPR of OFDM signals should be reduced as long as an efficient and economic operation of the entire OFDM signal processing circuitry is desired. Due to its low implementation complexity, low processing speed, and consequently, no bandwidth expansion, companding the ranges of largely swinging signals is one of the most popular PAPR reduction techniques in OFDM-based systems [8].

Reducing the PAPR allows the power consumption to be decreased by the power amplifier and the DAC on the transmitter while the average signal power needs to be kept constant. On the other hand, higher average signal power can be delivered with a set power source, thereby improving the total signal-to-noise ratio (SNR) and, as a result, the BER of the receiver. In addition, low PAPR allows the power amplifier to work at a bias point where non-linearity is minimal. Several approaches have been developed to resolve the high PAPR problem in OFDM. In [9], the authors introduced the $\mu-$law companding scheme. A closed-form of BER expression is proposed and validated with the Monte-Carlo simulation. However, this scheme reduced the PAPR at the expense of an increase in the average signal power, which causes a nonlinear distortion. The authors developed the exponential companding technique in [10]. It used a non-linear function to change the compressed signal to a uniform distribution. This scheme essentially reduced the PAPR and kept the average signal-power constant. However, this causes a relatively high signal distortion and spectrum side-lobes generation, which increases the BER.

In [11], a new type of companding was proposed depends on erf(.) function entitled new error function (NERF). The results show that the NERF companding technique provided better PAPR reduction and BER performance than the $\mu-$law method. A new nonlinear companding technique called "exponential companding" is proposed in [12]. The scheme modified both large and small signals and retained the average power at the same level. The exponential companding scheme essentially reduces the PAPR by converting the original OFDM signals into uniformly distributed signals. As well as the exponential companding scheme offers less spectrum side-lobes and better PAPR reductions and reduces the system BER. In [13], the authors suggested a non-linear companding function for the reduction of PAPR. The companding function converts the signals into a probability density function (PDF) with a cumulative distribution function (CDF) and an anti-trigonometric function. The Companding Scheme gave more design flexibility to meet the various design specifications. In addition, the BER performance is improved to less than 10^{-4} in the additive white Gaussian noise channel (AWGN) and QPSK modulation scheme. In [14], a selective mapping (SLM) and partial transmit sequence (PTS) schemes are proposed for mitigating the PAPR sing a low complexity
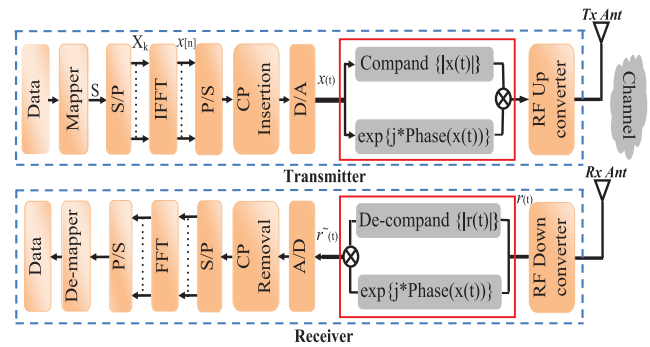

FIGURE 1. Block diagram of OFDM system with companding/de-companding schemes.

T-transform rather than inverse fast Fourier transform (IFFT). The combined T-transform with SLM reduces the computational complexity about 20% for $N = 128$ subcarriers than conventional schemes that use IFFT.

The remainder of this article is structured as follows. Section II offers a description of the general mathematical model of OFDM-based systems. Section III describes the consequences of non-linear power amplifiers. Section IV lays out the mathematical concept of the PAPR. Section V discusses the mathematical formulation of the proposed methodology (IMADJS) to reduce high PAPR. Section VI illustrates the computational complexity of the various companding strategies. Section VII introduces computational simulation results comparing well-known companding techniques such as $\mu-$law [15], AEXP [16], and NERF [11] with the proposed technique.

II. OFDM SYSTEM MODEL

Fig. 1 shows a generic block diagram of the OFDM transceiver sequence that involves a compandor and a de-compandor to minimize the PAPR. First, the input data is mapped using different mapping schemes, such as M-ary phase-shift keying (PSK) or quadrature amplitude modulation (QAM). (QAM). The S mapping data should be converted from serial to parallel depending on the number of sub-carriers. Suppose there are N sub-carriers in the OFDM system. They are indexed from $k = 0$ to $N - 1$. The S/P converter transforms the input data to the N parallel data stream. The complex symbols of the kth sub-carrier, $X_k, \{k = 0, 1, \ldots, N - 1\}$, will be transferred through IFFT block to get the OFDM signal. The OFDM signal is created by summing up the N modulated sub-carriers. Mathematically, the OFDM modulated signal can be expressed as [7], [17]:

$$x(t) = \sum_{k=0}^{N-1} X_k \cdot e^{j2\pi \frac{k}{NT_s}t}; \quad 0 \leq t \leq NT_s, \qquad (1)$$

where T_s and N represent the symbol duration, and the number of sub-carriers that constitute the OFDM signal, respectively. The discrete time base-band OFDM signal x_n sampled

at the Nyquist rate $t = nT_s$ can be defined as:

$$x_n = \sum_{k=0}^{N-1} X_k . e^{j2\pi \frac{nk}{N}}, \quad n = 0, 1, \ldots \ldots, N - 1. \quad (2)$$

The mapped data X_k is processed by an inverse discrete Fourier transform (IDFT). A parallel-to-serial (P/S) converter is applied to the resulting time-domain symbols $x(n)$. In order to overcome the ISI problem, the cyclic prefix (CP) is used in the OFDM symbol. Also, to prevent the clipping-induced non-linearities introduced by the HPA, a companding operator denoted by $f(.)$, is added to the amplitude of the signal $|x(t)|$ to maintain the output signal phases unchanged. Finally, the signal is amplified to the desired power level using a power amplifier and transmitted over the communication channel.

III. NON-LINEAR POWER AMPLIFIER AND PAPR

The high PAPR of OFDM requires system components with a large linear power amplifier (PA) range capable of accommodating the signal. Otherwise, the nonlinear distortion occurs, which results in a loss of sub-carrier orthogonality, and degrades the performance. In practice, the PA has a limited linear region, beyond which it saturates to a maximum output level. The amplitude and phase characteristics of the PA are given by [18], [19]:

$$A_{PA}(|s(t)|) = \frac{G_0 |s(t)|}{\left(1 + \left(\frac{|s(t)|}{A_{sat}}\right)^{2p}\right)^{\frac{1}{2p}}}, \quad (3)$$

$$\phi_{PA}(|s(t)|) = 0. \quad (4)$$

where G_0 is the amplifier gain, A_{sat} is the input saturation level, P controls the sharpness Furthermore, the PAPR measured in dB is expressed as follows [7]:

$$PAPR\{x(n)\}(dB) = 10. \log_{10} \left(\frac{\max |x(n)|^2}{E\{|x(n)|^2\}}\right). \quad (5)$$

where, $E\{.\}$ is the statistical expectation operator, $\max |x(n)|^2$ is the peak OFDM signal power and $E\{|x(n)|^2\}$ is the average power of the OFDM signal.

IV. MATHEMATICAL FORMULATION OF THE PROPOSED COMPANDING TECHNIQUE

The proposed technique (IMADJS) is based on intensity transformation function. This function is defined as [20]:

$$f(x) = \begin{cases} c & \text{if } x \leq a, \\ \left(\left(\frac{x-a}{b-a}\right)^\gamma (d-c) + c\right) & \text{if } a < x < b, \quad (6) \\ d & \text{if } x \geq b. \end{cases}$$

where, a is low input of the signal x, b is high input of the signal x, c is low output of the signal x, d is high output of the signal x and γ is a positive number uses as a degree of companding.

This function maps the intensity values in signal f to new values in another signal g, such that values between low-input and high-input map to values between low-output and high-output. Values under low-input and over high-input are clipped; that is, values under the low-input map to low-output, and those over the high-input map to high-output [21]. The OFDM signal companding function Eq. (6) is used by the proposed companding technique to minimize high PAPR. This equation is used to find a linear function that preserves a stable average power level (i.e., average power before companding is nearly the same after companding). We assume that if the low-input signal a happens when there is no signal at all, the low output c is not a signal. The means that:

$$\begin{aligned} a = 0, \quad b = 0, \\ 0 \leq f(x) \leq d. \quad (7) \end{aligned}$$

where, x is the input signal and $f(x)$ is the output signal. Also, the aim of the proposed function is to scale the input x with respect to the high input b and high output d, when $x \in]0, b[$ and $f(x) \in [0, d]$. This aim is satisfied when:

$$\begin{aligned} \gamma = 1, \\ 0 < x < b, \quad 0 \leq f(x) \leq d, \\ b \neq d. \quad (8) \end{aligned}$$

By substitution from Eq. (7), and Eq. (8) in Eq. (6), we obtain the IMADJS linear function as follows:

$$f(x) = \begin{cases} 0 & \text{if } x \leq 0, \\ \frac{xd}{b} & \text{if } 0 < x < b, \quad (9) \\ d & \text{if } x \geq b. \end{cases}$$

where, a is low-input of the signal x, b is high-input of the signal x, c is low-output of the signal x, d is high-output of the signal x.

Fig. 2 compares the performance of the proposed transfer function by Eq. (6) and the performance of transfer function defined by Eq. (9) for different values of γ. It is clear that, due to the linearity of the proposed function defined by Eq. (9), where $\gamma = 1$, the performance of the proposed technique will be more efficient compared with the other models for which $\gamma \neq 1$. However, the values less than one produce a function which is concave downward. Decreasing *high-in* parameter compresses large signals, while the *high-out* parameter adjusts small signals. In this article, the value of *low-input* and *low-output* are fixed to zero, because the minimum degradation in BER is achieved at these values (*low-in* = 0 and *low-out* = 0), as it will be explained in details in simulation section.

V. COMPANDING ALGORITHMS AND COMPUTATIONAL COMPLEXITY ANALYSIS

This section describes the algorithms used for the comparative study of the four companding techniques. Algorithm 1 is designed to simulate the transmitter part; Algorithm 2 is developed for the receiver part, while Algorithm 3 and
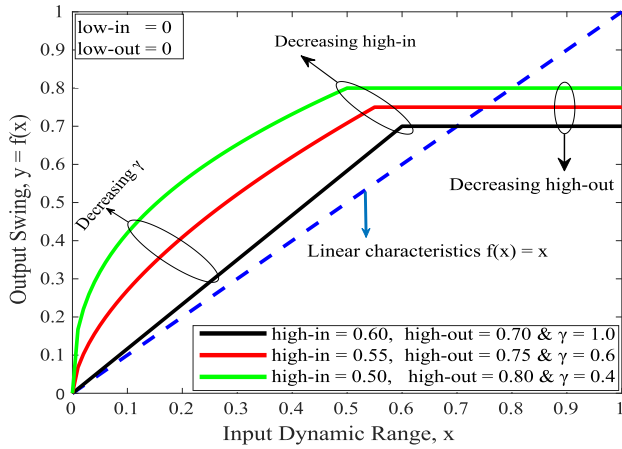
FIGURE 2. IMADJS transfer function.

TABLE 1. Computational complexity of various companding techniques.

Algorithm	Additions	Multiplications	FFT
μ-law	N	$5N$	$N\log_2 N$
NERF	$(1 + 2K_1/K_2)N$	$3(1 + K_1/K_2)N$	Additions &
AEXP	$3N$	$6N$	$\frac{N}{2}\log_2 N$
IMADJS	N	$2N$	Multiplications

Algorithm 4 represent the companding and decompanding for different techniques. The complexity of the algorithms is determined by using the models of the research represented in [22]–[24]. The complexity calculations are considered under the following assumptions:

1) The complexity of addition is equal to the complexity of subtraction,
2) The complexity of multiplication matches the complexity of division,
3) Ignoring the complexity of abs, max, and compare functions,
4) Exponential function requires two multiplications and one addition,
5) erf(t) function requires $2t$ multiplications and $2t$ additions,
6) In AEXP companding technique, we assumed $d = 2$.

The number of additions, multiplications, and FFT operations assuming only *one* iteration for the four algorithms is summarised in Table 1. As shown, the number of the two types of computations in IMADJS and μ-law companding techniques are smaller than those in NERF and AEXP companding techniques. In addition, all techniques have the same complexity in FFT where they are using the same OFDM transmitter and receiver. The FFT complexity equals $N \log_2 N$ for additions and $(N/2) \log_2 N$ for multiplications.

VI. SIMULATION RESULTS AND DISCUSSION

This section discusses the numerical simulation and results for the OFDM system using the new companding technique (IMADJS). For contrast, well-known conventional PAPR reduction techniques such as μ-law companding technique [15], new error function (NERF) [11] and Absolute

Algorithm 1 The Transmitter

1: PAPR = zeros $(1, n)$; $\rightarrow$ n is the number of subcarrier,
2: Tx = [ ];
3: Generated data (S) is converted from serial to parallel (Matrix form) based on the type of modulation and the number of subcarrier (n).
4: **for** $i = 2 : n - 1$ **do**
5:     $X(i) = $ QAM (S); $\rightarrow$ Modulation
6:     $x(i) = $ **IFFT**$(X(i))$; $\rightarrow$ Convert to time domain
7:     $x(i) = x(i) + $ **cp**; $\rightarrow$ Add cyclic prefix
8:     $x_{\text{comp}} = $ Compand $(|x(i)| \times $ phase$(x(i))$; $\rightarrow$ Companding function
9:     $x_{\text{amp}} = $ **SSPA**(x_{comp}); $\rightarrow$ Apply SSPA Amplifier
10:    Peak-power $= $ **max**$(|x_{\text{comp}}|^2)$;
11:    Avg-power $= $ **mean**$(|x_{\text{comp}}|^2)$;
12:    PAPR$(i) = 10 \times \log_{10}$(Peak-power/Avg-power);
13:    Tx = [Tx x_{amp}];
14: **end for**
15: Pilot = zeros $(1, $ length $(x(i)))$;
16: y = [pilot   Tx   pilot]; $\rightarrow$ Transmitted signal

Algorithm 2 The Receiver

1: Output = [ ];
2: **for** $j = 1 : $ length(snr) **do**
3:     $r_x = y+ $ noise; $\rightarrow$ Received under Rayleigh fading channel
4:     **for** $k = 2 : n - 1$ **do**
5:         $r_{\text{Decomp}} = $ De-compand $(|r_x(k)| \times $ phase$(r_x(k))$; $\rightarrow$ Decompanding function
6:         $r_{cp} = $ RemoveCP(r_{Decomp}); $\rightarrow$ Remove cyclic prefix
7:         $R_x = $ **FFT**(r_{cp}); $\rightarrow$ Convert to frequency domain
8:         $R_{Eq} = R_x/G(j)$; $\rightarrow$ Equalization with gain $G(j)$
9:         Data $= $ **QAM**$_{\text{demod}}(R_{Eq})$;
10:        Output = [Output   Data];
11:    **end for**
12:    Error $= $ BER $(y, $ Output$)$; $\rightarrow$ BER calculation
13: **end for**

exponential (AEXP) companding technique [16] are considered. Improvement in PAPR, degradation in BER, average power, and spectral density (PSD) are used as performance metrics of interest. The improvement in PAPR is the difference between the PAPR of the original signal and the PAPR of the companding signal (*i.e.* Improvement in PAPR = PAPR of original signal - PAPR of companding signal). Similarly, the degradation in BER is the difference between the BER of the original signal and the BER of the companding signal. Table (2) lists the used simulation parameters of the system.

A. SIMULATION RESULTS OF THE PROPOSED IMADJS TECHNIQUE

This section shows the effect of changing the parameters of the IMADJS technique on PAPR and BER. The IMADJS

Algorithm 3 Companding Techniques

   μ-law Companding Technique

1: $B = \text{abs}(X)$;
2: $V = \max(B)$;
3: $C = \mu \times B/V$;
4: $f(X) = \frac{V}{\mu} \times C \times \text{sgn}(X)$;

   NERF Companding Technique

1: $K_1 = \text{abs}(X)$;
2: $K_2 = \sqrt{2}\,\sigma$;
3: $f(X) = \sqrt{3}\,\sigma \times \text{erf}(K_1/K_2) \times \text{sgn}(X)$;

   AEXP Companding Technique

1: $A = \text{abs}(X)$;
2: $B = \text{mean}(A)$;
3: $C = \exp(-A/\sigma^2)$;
4: $E = [(1 - C)^2]^{1/d}$;
5: $\alpha = [B/\text{mean}(E)]^{d/2}$;
6: $f(X) = \alpha \times (1 - C)^{1/d} \times \text{sgn}(X)$;

   IMADJS Companding Technique

1: $n = \text{length}(x)$;
2: **for** $i = 1 : n$ **do**
3:    **if** $x(i) \leq a$ $\rightarrow a$ is low input **then**
4:      $y(i) = c$; $\rightarrow c$ is low output
5:    **else if** $x(i) \geq b$ $\rightarrow b$ is high input **then**
6:      $y(i) = d$; $\rightarrow d$ is high output
7:    **else**
8:      $y(i) = x(i) \times d/b$
9:    **end if**
10: **end for**

Algorithm 4 Decompanding Techniques

   μ-law Companding Technique

1: $B = \text{abs}(X)$;
2: $V = \max(B)$;
3: $C = \mu \times B/V$;
4: $f^{-1}(X) = \frac{V}{\mu} \times C \times \text{sgn}(X)$;

   NERF Companding Technique

1: $K_1 = \text{abs}(X)$;
2: $K_2 = \sqrt{3}\,\sigma$;
3: $f^{-1}(X) = \sqrt{2}\,\sigma \times \text{erf}^{-1}(K_1/K_2) \times \text{sgn}(X)$;

   AEXP Companding Technique

1: $A = \text{abs}(X)$;
2: $B = \text{mean}(A)$;
3: $C = \exp(-A/\sigma^2)$;
4: $E = [(1 - C)^2]^{1/d}$;
5: $\alpha = [B/\text{mean}(E)]^{d/2}$;
6: $f^{-1}(X) = \sqrt{(-\sigma^2 \times \log_e \times (1 - G/\alpha))} \times \text{sgn}(X)$;

   IMADJS Companding Technique

1: $n = \text{length}(x)$;
2: **for** $i = 1 : n$ **do**
3:    **if** $x(i) \leq c$ $\rightarrow a$ is low output **then**
4:      $y(i) = a$; $\rightarrow c$ is low input
5:    **else if** $x(i) \geq d$ $\rightarrow b$ is high output **then**
6:      $y(i) = b$; $\rightarrow d$ is high input
7:    **else**
8:      $y(i) = x(i) \times b/d$
9:    **end if**
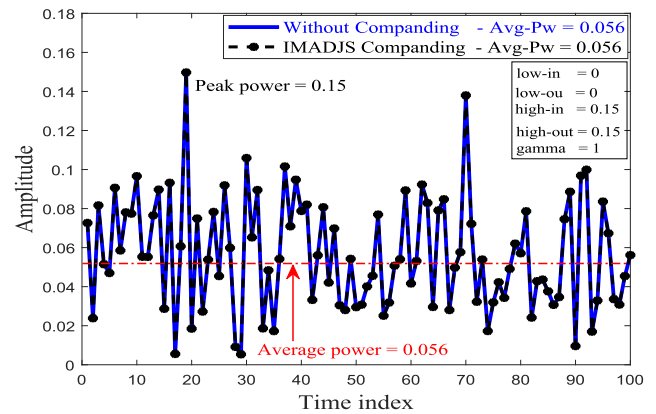10: **end for**

TABLE 2. Simulation parameters.

Parameter	Value and Unit
Spacing frequency, Δf	15 kHz
Sampling frequency , f_s	3.84 MHz
Number of symbols	1000 symbols
FFT size, N	256
CP length, N_{CP}	64 samples
Modulation type	QPSK, 4-QAM, 16-QAM and 64-QAM
Channel model	AWGN and Rayleigh fading channel
Power amplifier model (PA)	SSPA (p = 2, G_0 = 1 and A_{sat} = 1)

FIGURE 3. An OFDM signal with high PAPR without and with IMADJS companding.

technique has five parameters (*low-in, high-in, low-out, high-out* and γ). Each parameter will be analyzed separately to show its effect on PAPR reduction and BER performance. We investigate the effects of changing the IMADJS parameters on PAPR and BER. As a result, the IMADJS parameters are configured as follows: *low-in* $= 0$, *low-out* $= 0$, *high-in* $= 0.15$, *high-out* $= 0.15$ and $\gamma = 1$. It is clear from Fig. 3 that, the received OFDM signal without and with the proposed IMADJS companding technique.

1) THE EFFECT OF CHANGING THE *low-in* PARAMETER

To study the effect of *low-in* parameter on the PAPR and BER, the *low-in* parameter increases by small value

(*low-in* $= 0 : 0.0015 : 0.15$) to demonstrate the effect of increasing this parameter on the PAPR reduction and BER results. The improvement in the *low-in* parameter leads to an increase in the PAPR and a decreasing in the BER. It is observed that the best value for the *low-in* parameter is zero, where the less PAPR and less degradation in BER are achieved at this value (*low-in* $= 0$).

Fig. 4 shows the transfer function of IMADJS technique with increasing the *low-in* parameter. Three values for *low-in*
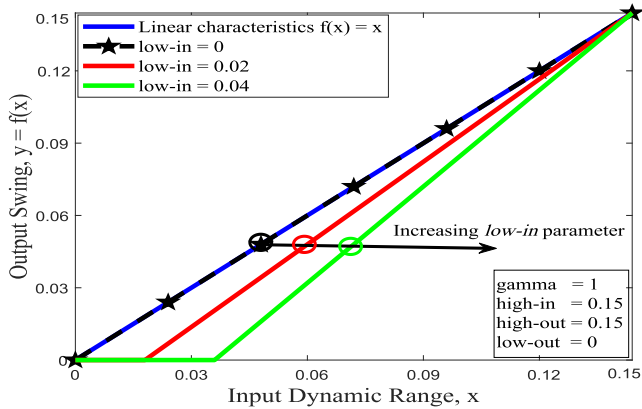
FIGURE 4. Transfer function of IMADJS companding technique with the changing of *low-in* parameter.

FIGURE 5. Transfer function of IMADJS companding technique with the changing of *low-out* parameter.

parameter (*low-in* = 0; 0.02; 0.04) are considered and the rest parameters are fixed (*low-out* = 0, *high-in* = 0.15, *high-out* = 0.15 and γ = 1), as shown in Fig. 4. When the *low-in* parameter is zero (*low-in* = 0), the curve of IMADJS technique (black curve) is identical to the curve of linear characteristic function {blue cure, $f(x) = x$}. Thus, there is neither an improvement in PAPR nor degradation in BER, because the input signal is equal to the output signal. Increasing the *low-in* parameter leads to compress the small signals and keeps the peak of the signal unchanged, as it is seen with the two curves (red and green) in Fig. 4. Decreasing small signals leads to decrease the average power of the signal. Consequently, increasing the PAPR and the degradation in BER. Based on the above, the optimum value of *low-in* parameter is zero.

2) THE EFFECT OF CHANGING THE *low-out* PARAMETER
To present the effect of the *low-out* parameter on the PAPR and BER, the *low-out* parameter increases by a small value (*low-out* = 0 : 0.0015 : 0.15) to show the effect of increasing this parameter on the PAPR reduction and BER performance. The improvement in PAPR increases by increasing the *low-out* parameter. However, this improvement in PAPR leads to an increase in BER. Fig. 5 shows the transfer function of IMADJS technique when the *low-out* parameter increases. Three values for *low-out* parameter (*low-out* = 0; 0.025; 0.050) are considered and the rest parameters are fixed (*low-in* = 0, *high-in* = 0.15, *high-out* = 0.15 and γ = 1), as shown in Fig. 5. When the *low-out* parameter is zero (*low-out* = 0), the curve of IMADJS technique (red curve) is identical to the curve of linear characteristic function {blue cure, $f(x) = x$}. Thus, there is neither an improvement in PAPR nor degradation in BER, because the input signal is equal to the output signal. Increasing *low-out* parameter leads to enlarge small signals and keeps the peak of the signal unchanged, as it is seen with the two curves (green and black) in Fig. 5. Increasing the *low-out* parameter leads to increase the average power of the signal, which leads to increase the improvement in PAPR and the degradation in BER.
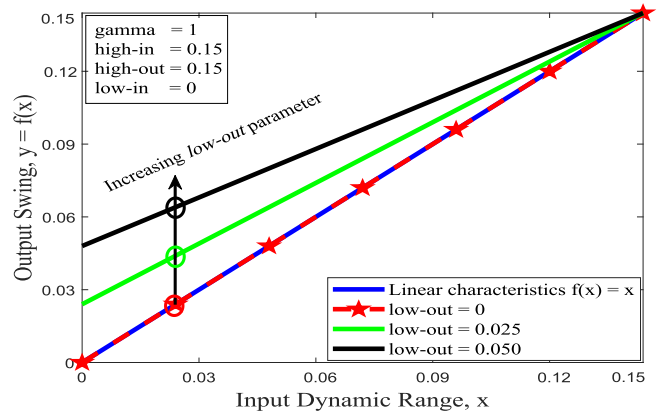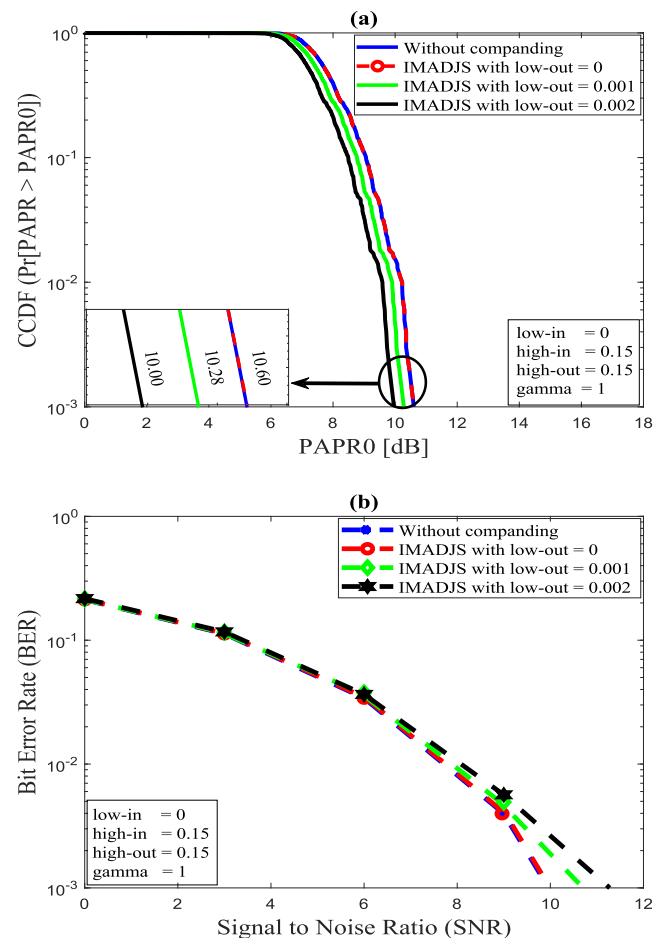

FIGURE 6. IMADJS technique with the change of *low-out* parameter: (a) PAPR and (b) BER.

Fig. 6 shows the improvement in PAPR and degradation in BER for three values of *low-out* parameter in IMADJS technique. Fig. 6(a) displays the improvement in PAPR with four fix parameters (*low-in* = 0, *high-in* = 0.15, *high-out* = 0.15 and γ = 1) and three values for the *low-out* parameter. At *low-out* = 0, there is no companding (the signal before and after companding is the same). Increasing the *low-out*
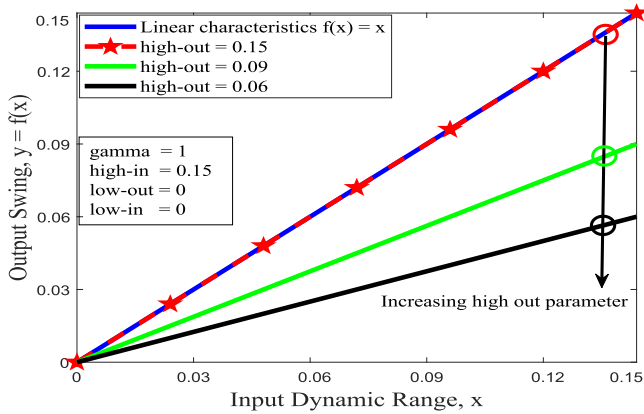
FIGURE 7. Transfer function of IMADJS companding technique with different *high-out* parameter.

FIGURE 8. Transfer function of IMADJS companding technique with different *high-in* parameter.

parameter leads to increase the small signals, which cause to increase the average power; therefore, decreasing the PAPR. Increasing the *low-out* parameter by a small value (0.001 and 0.002) leads to negligible improvement in PAPR (0.32dB, 0.60dB), as seen in Fig. 6(a). However, this improvement is accompanied by deterioration in the BER performance, as shown in Fig. 6(b). In order to achieve the same BER (10^{-3}) of the original OFDM signal (without companding), the required SNRs are about 10.5dB at *low-out* = 0.001 and 11dB at *low-out* = 0.002. Accordingly, the degradation in BER is large compared to the improvement in PAPR. Based on the above, the best choice for *low-out* parameter is zero. Where at *low-out* = 0, the improvement in PAPR is zero and the degradation in BER is zero as well.

3) THE EFFECT OF CHANGING THE *high-out* PARAMETER
To demonstrate the effect of changing the *high-out* parameter on the PAPR and BER, the *high-out* parameter adjusts by small value (*high-out* = 0.0015 : 0.0015 : 0.15) to see the effect of altering this parameter on the PAPR and BER. Fig. 7 shows the transfer function of IMADJS technique when the *high-out* parameter decreases. Three values for *high-out* parameter (*high-out* = 0; 0.025; 0.050) are considered and the rest parameters are fixed as follows: *low-in* = 0, *high-in* = 0.15, *low-out* = 0 and γ = 1, as shown in Fig. 7. At *high-out* = 0.15, the curve after companding (red curve) is identical to the curve before companding (blue curve) and this means there is no companding. Decreasing the *high-out* parameter leads to do scaling for the input signal (compress all the signal by the same level), as it is clear in the two curves green and black in Fig. 7. Consequently, this is the reason that the PAPR and BER are unchanged, although the *high-out* parameter decreases.

4) THE EFFECT OF CHANGING THE *high-in* PARAMETER
The effect of *high-in* parameter on the PAPR and BER is shown in Fig. 8. The *high-in* parameter changes by small value (*high-in* = 0.0015 : 0.0015 : 0.15) to show the effect of decreasing this parameter on the PAPR reduction and
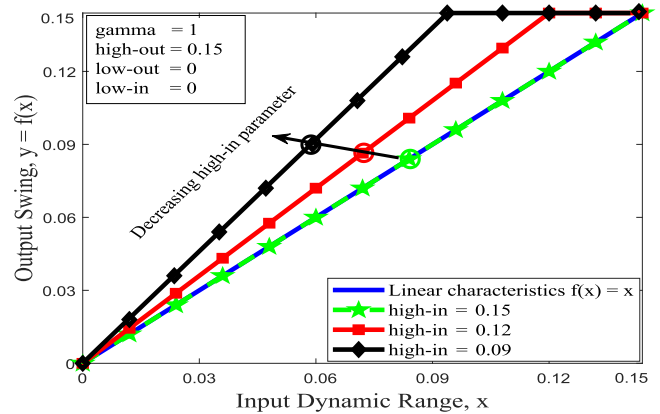
BER performance. Decreasing the *high-in* parameter leads to a decrease in the PAPR and increasing the improvement in PAPR. For the BER, decreasing the *high-in* parameter increases the degradation in BER increases. Thus, there is a trade-off between the improvement in PAPR and the degradation in BER.

5) THE EFFECT OF CHANGING THE DEGREE OF COMPANDING (γ)
The effect of changing the degree of companding (γ) on the PAPR and BER in the IMADJS technique is presented in Fig. 9 when γ changes as (γ = 0 : 0.02 : 2). The PAPR of the original signal (before companding) is 11.49 (10.6dB) and the PAPR of companding signal with γ = 1 is 11.49 as well. The PAPR decreases when the parameter γ less than 1 because the small signals are enlarged with γ < 1. However, PAPR increases when γ > 1 as seen in Fig. 9(a). Furthermore, the BER increases when the parameter γ less than or greater than 1, as shown in Fig. 9(b).

Fig. 9 uses to obtain the optimal value of γ. As can be seen, the minimum value of BER can be achieved when γ = 1. As well Fig. 10 confirms this optimal value whereas it also gives the minimum PAPR. Additionally, Fig. 11 shows the transfer function of IMADJS technique for different values of γ (γ = 0.5, γ = 0.8, γ = 1.0, γ = 1.5 and γ = 2.0) and four fix parameters (*low-in* = *low-out* = 0 and *high-in* = *high-out* = 0.15). For γ = 1.0, the signal after companding is equal to the signal before companding. Decreasing γ (γ < 1) leads to enlarge small signals and keep the peak of the signal unchanged, as shown in Fig. 11. Consequently, the improvement in PAPR increases, as shown in Fig. 9(a). Increasing γ (γ > 1) leads to compress small signals and keep the peak of the signal unchanged, as seen in Fig. 11. Therefore, this leads to increase the PAPR, as shown in Fig. 9(a). Distorting signal (increasing or decreasing γ) leads to increase the degradation in BER, as shown in Fig. 9(b).

B. PERFORMANCE COMPARISON BY USING RAYLEIGH FADING CHANNEL
This section presents a performance comparison of companding-based PAPR suppression techniques using
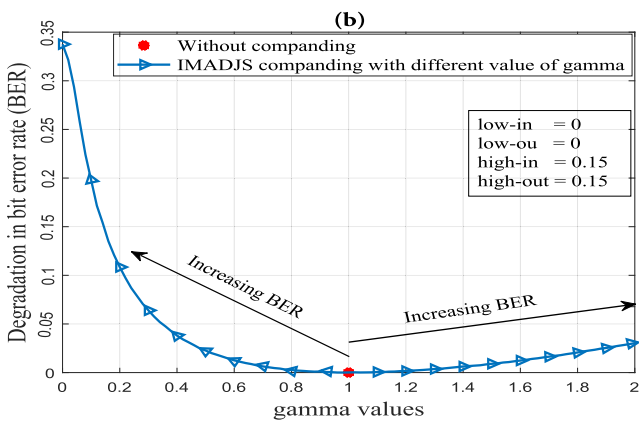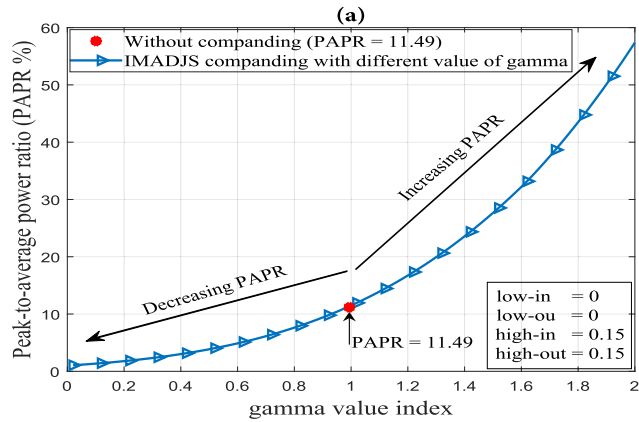
FIGURE 9. Effect of decreasing the γ value in the IMADJS technique on (a): PAPR and (b): BER.
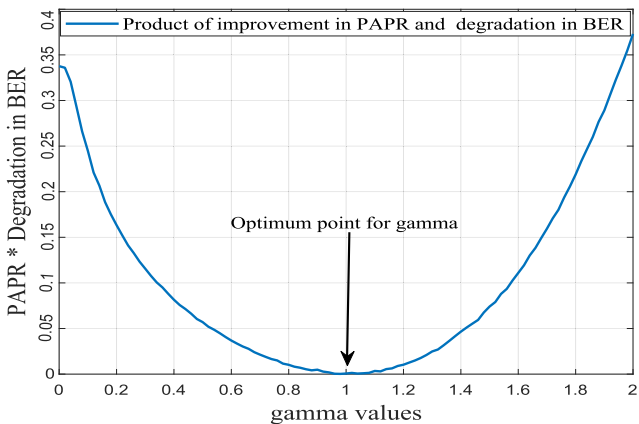

FIGURE 10. Product of the PAPR curve and the BER curve.

Rayleigh Fading Channel, QPSK Modulation, and different M-QAM Modulation techniques (4-QAM, 16-QAM, and 64-QAM). The various companding techniques are compared using a multi-path channel. The Rural-Urban channel (COST207) with a 6 path is used as a multi-path channel. Table 3 shows the power and delay of the channel, according to COST207. The NERF companding technique is used as a reference for a PAPR reduction and BER performance. In comparison to other companding techniques, the NERF
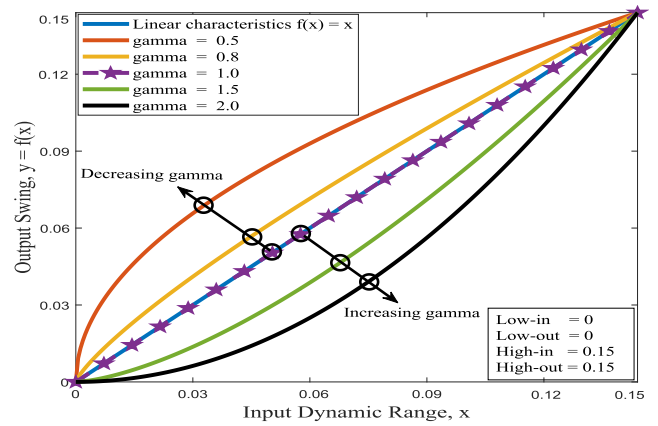

FIGURE 11. Transfer function of IMADJS technique with the change of γ parameter.

TABLE 3. Channel power-delay profile [25].

| Rural Urban channel (COST207)						
Tap number	1	2	3	4	5	6
Power (dB)	0	-4	-8	-12	-16	-20
Delay (μs)	0	0.1	0.2	0.3	0.4	0.5

companding technique produces one value for PAPR and one value for BER. Consequently, to achieve an equal distinction of all techniques, the conditions of all techniques are set to obtain the same PAPR as the NERF companding technique. The performance of the BER will then be compared to the various companding techniques.

1) COMPARING IMADJS TECHNIQUE WITH THE EXISTING COMPANDING TECHNIQUES BASED ON THE AVERAGE POWER

This section presents the average power (Avg-pw) simulation results for the original signal (without companding) versus the companding signal using μ-law, AEXP, NERF, and IMADJS companding techniques. To get a fair comparison, the parameters for all techniques are changed to obtain similar PAPR results for all techniques, where $d = 1.3$, $\mu = 28$, *low-in* $= 0$, *low-out* $= 0$, $\gamma = 1$, *high-in* $= 0.093$ and *high-out* $= 0.1$. According to these parameters and by using the QPSK modulation, the average power (Avg-pw) for all techniques is portrayed in Fig. 12. As shown, the average power for IMADJS, AEXP, and NERF companding techniques is similar to the average power of the original signal. However, the μ-law companding scheme raises the average companding signal power. Therefore, the μ-law companding technique offers an increase in BER more than in others.
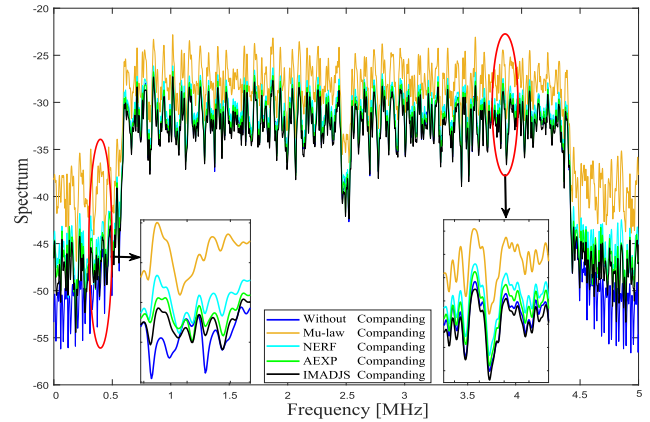
2) COMPARING IMADJS TECHNIQUE WITH THE EXISTING COMPANDING TECHNIQUES BASED ON PSD

Fig. 13 shows the PSD of μ-law, AEXP, NERF, and IMADJS companding techniques. It can be seen that the companded signals by using the IMADJS technique have
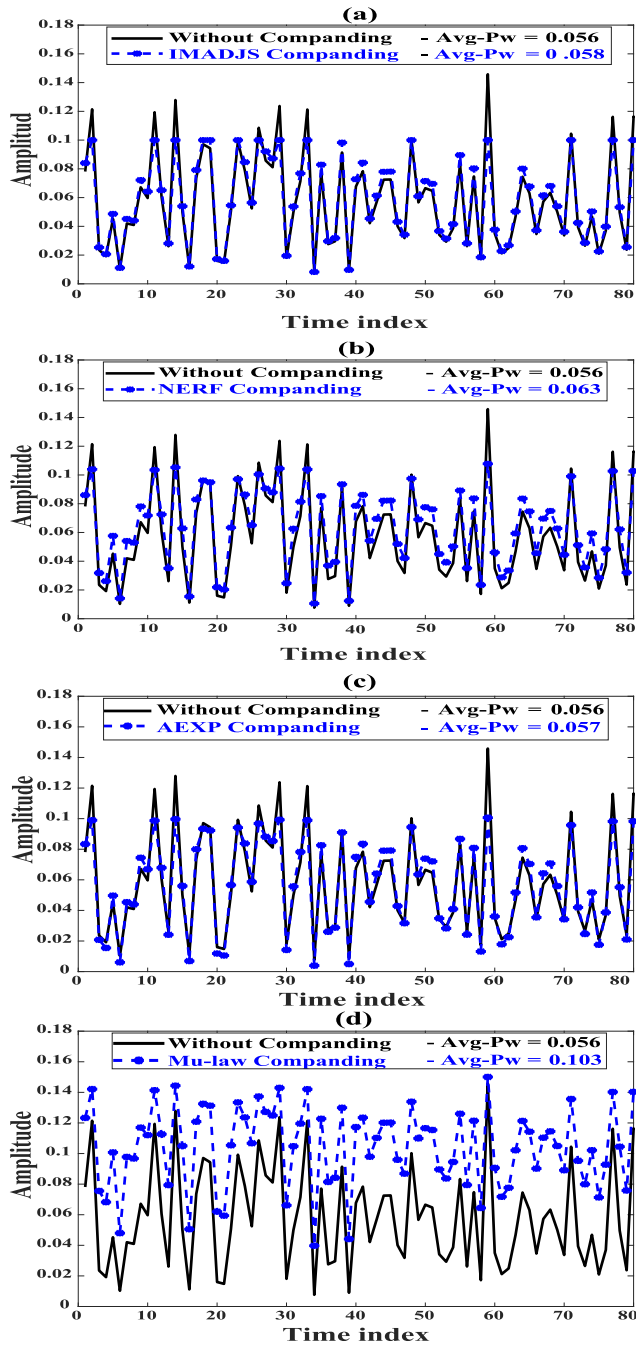
FIGURE 12. Comparing the different companding techniques based on the average power: (a) IMADJS technique, (b) NERF technique, (c) AEXP technique and (d) μ-law technique.

FIGURE 13. PSD of Original signal versus companded signals by using different companding techniques: μ-law, NERF, AEXP and IMADJS.

a spectrum characteristic nearly to the original signal (no spectral regrowth) compared with the other techniques, which increase the PSD of the companded signal for PAPR reduction. As shown in Fig. 13, he μ-law companding scheme contains a high out-of-band component, and the processed signals by the new scheme (IMADJS) have less out-of-band radiation. The average of out-of-band radiation in IMADJS technique reaches about −50dB at the frequency 0 MHz, the AEXP and NERF companding techniques reach about −46dB, while the μ-law companding technique reaches

about −37 dB at the frequency 0 MHz. It is the leading cause that the IMADJS technique increases the small amplitude signals and compresses the large amplitude signals while keeping the average power unchanged, increasing the resistance of small amplitude signals from noise. The AEXP, NERF, and IMADJS companding techniques have the same principle, where all three techniques increase the small amplitude signals and compress the high amplitude signals. Consequently, they keep the average power before and after companding unchanged. However, the μ-law companding technique increases the average power level and does not change the peak of signals; therefore, the linear operation region in HPA should be larger when the same system performances are requested.

3) COMPARING IMADJS TECHNIQUE WITH THE EXISTING COMPANDING TECHNIQUES BASED ON THE BER

In this section, the proposed (IMADJS) technique is compared with μ-law, AEXP, and NERF companding techniques, based on the PAPR and BER M-QAM modulation scheme ($M = 4, 16$ and 64). In order to get a fair comparison, the parameters for all techniques are changed carefully to obtain the same PAPR of NERF companding technique, as seen in Fig. 14. Furthermore, the degree of companding for AEXP technique is 1.3 ($d = 1.3$) and the μ-law parameter is 28 ($\mu = 28$). For the IMADJS technique, the parameters are set as *low-in* = 0, *low-out* = 0, and $\gamma = 1$.

In 4-QAM, the NERF companding technique gives a reference PAPR at 4.37 dB (see Fig. 14(a)) and the rest of IMADJS parameters are configured as *high-in* = 0.13, *high-out* = 0.145. The BER versus the SNR is presented in Fig. 14(b). As seen, the proposed (IMADJS) technique gives the lowest value of BER compared to the other techniques. In 16-QAM, the NERF companding technique gives a reference PAPR at 4.35 dB (see Fig. 14(c)) and the rest of IMADJS parameters are configured as *high-in* = 0.29, *high-out* = 0.31. The BER versus the SNR is presented in Fig. 14(d). As seen, the proposed (IMADJS) technique gives the lowest value of BER compared to the other techniques. In 64-QAM, the NERF
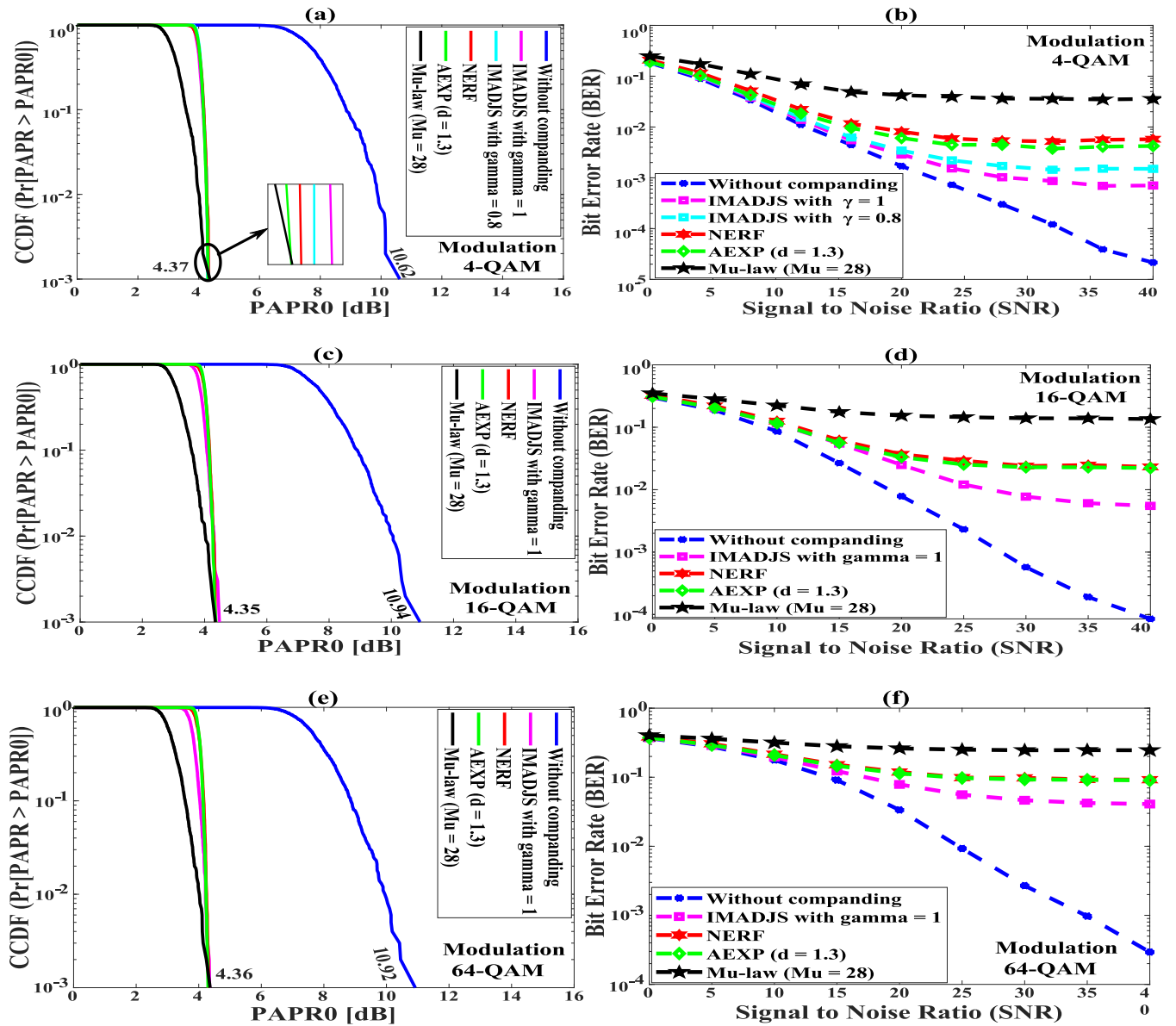
FIGURE 14. Comparing the different companding techniques based on BER when all techniques have same PAPR: (a) same PAPR with 4-QAM, (b) BER with 4-QAM, (c) same PAPR with 16-QAM, (d) BER with 16-QAM, (e) same PAPR with 64-QAM and (f) BER with 64-QAM.

TABLE 4. Comparison for different companding techniques based on: PAPR, BER, Avg-pw and PSD.

	Modulation	Original signal	IMADJS	AEXP	NERF	μ-law	Figure
The PAPR at CCDF = 10^{-3}	4-QAM	PAPR = 10.62	PAPR = 4.37	PAPR = 4.37	PAPR = 4.37	PAPR = 4.37	Fig. 14(a)
The BER at SNR = 40 dB	4-QAM	BER = $2.2*10^{-5}$	BER = $7*10^{-4}$	BER = $4.2*10^{-3}$	BER = $5.7*10^{-3}$	BER = $3.6*10^{-2}$	Fig. 14(b)
The PAPR at CCDF = 10^{-3}	16-QAM	PAPR = 10.94	PAPR = 4.35	PAPR = 4.35	PAPR = 4.35	PAPR = 4.35	Fig. 14(c)
The BER at SNR = 40 dB	16-QAM	BER = $8.5*10^{-5}$	BER = $5.5*10^{-3}$	BER = $2.2*10^{-2}$	BER = $2.2*10^{-2}$	BER = $13.5*10^{-2}$	Fig. 14(d)
The PAPR at CCDF = 10^{-3}	64-QAM	PAPR = 10.92	PAPR = 4.36	PAPR = 4.36	PAPR = 4.36	PAPR = 4.36	Fig. 14(e)
The BER at SNR = 40 dB	64-QAM	BER = $2.9*10^{-4}$	BER = $4*10^{-2}$	BER = $9*10^{-2}$	BER = $9*10^{-2}$	BER = $24.5*10^{-2}$	Fig. 14(f)
The average power	QPSK	Avg-pw = 0.056	Avg-pw = 0.058	Avg-pw = 0.057	Avg-pw = 0.063	Avg-pw = 0.103	Fig. 12
PSD at 0 MHZ	4-QAM	PSD = - 52 dB	PSD = - 50 dB	PSD = - 46 dB	PSD = - 46 dB	PSD = - 37 dB	Fig. 13

companding technique gives a reference PAPR at 4.36 dB (see Fig. 14(e)) and the rest of IMADJS parameters are

configured as *high-in* = 0.59, *high-out* = 0.59. The BER versus the SNR is presented in Fig. 14(f). As seen, the

proposed (IMADJS) technique gives the lowest value of BER compared to the other techniques. The μ-law companding technique has the maximum BER. The μ-law companding technique enlarges the small signals and keeps the peak of the signal unchanged. Accordingly, the resulting companded signals possess high average power levels. However, the increase in the average power of the companded OFDM signals is accompanied by increasing the BER.

VII. CONCLUSION

A new companding technique is used in this article to reduce the effects of high PAPR. The proposed technique, called (IMADJS) operates with a linear dynamic range and a nonlinear dynamic range. The IMADJS technique adjusts the small and large amplitude simultaneously while maintaining the same average power level before and after companding. The first simulation part shows the effect of changing the IMADJS parameters. The IMADJS has five parameters (*low-in, low-out, high-in, high-out* and γ). The impact of each parameter on PAPR and BER has been analyzed separately. The optimal value for the *low-in* parameter is zero (*low-in* = 0) and the *low-out* parameter is zero (*low-out* = 0). As with the *high-in* and *high-out* parameters, reducing the *high-in* parameter limits large signals while changing the *high-out* parameter modifies small signals. A decrease follows this improvement in the performance of the BER. Based on the above, there is always a trade-off between PAPR improvement and BER degradation. The optimal value for γ is 1 for the degree of companding (γ).

The second part of the simulation conducted a comparative analysis between the well-known companding techniques and the proposed technique (IMADJS) using the Rayleigh fading channel. The comparative analysis was based on PAPR improvement, BER degradation, average power (Avg-pw), and power spectral density (PSD). Table 4 concludes the performance comparison between the proposed technique (IMADJS) and the well-known companding techniques, such as μ-law, AEXP, and NERF companding techniques. For the same PAPR for all techniques, the minimum BER is obtained from the IMADJS technique, then the AEXP and NERF companding techniques. The maximum BER is reached with the use of the μ−law companding technique. For the average power of the companding techniques, the IMADJS, AEXP, and NERF companding techniques have about the same average power level as the initial OFDM signal. However, the μ-law companding technique does not maintain the average power before and after companding. Eventually, increasing the average power distorts the constellation points and allows small points similar to the large ones. As a result, the BER increases as the constellation points get closer. As for the PSD, the IMADJS technique has a lower effect on the original power spectrum relative to the other companding schemes.

REFERENCES

[1] T. Hwang, C. Yang, G. Wu, S. Li, and G. Ye Li, "OFDM and its wireless applications: A survey," *IEEE Trans. Veh. Technol.*, vol. 58, no. 4, pp. 1673–1694, May 2009.

[2] Y. Wu and W. Y. Zou, "Orthogonal frequency division multiplexing: A multi-carrier modulation scheme," *IEEE Trans. Consum. Electron.*, vol. 41, no. 3, pp. 392–399, Aug. 1995.

[3] W. Y. Zou and Y. Wu, "COFDM: An overview," *IEEE Trans. Broadcast.*, vol. 41, no. 1, pp. 1–8, Mar. 1995.

[4] R. Nee and R. Prasad, "OFDM for wireless multimedia communications. Artech house, 2000. Terrestrial radio access (EUTRA)," *Multiplexing Channel Coding*, pp. 562–573, Dec. 2018

[5] H. Schulze and C. Lüders, *Theory and Applications of OFDM and CDMA: Wideband Wireless Communications.* Hoboken, NJ, USA: Wiley, 2005.

[6] R. Prasad, *OFDM for Wireless Communications Systems.* Norwood, MA, USA: Artech House, 2004.

[7] D.-W. Lim, S.-J. Heo, and J.-S. No, "An overview of peak-to-average power ratio reduction schemes for OFDM signals," *J. Commun. Netw.*, vol. 11, no. 3, pp. 229–239, Jun. 2009.

[8] T. Jiang and Y. Wu, "An overview: Peak-to-average power ratio reduction techniques for OFDM signals," *IEEE Trans. Broadcast.*, vol. 54, no. 2, pp. 257–268, Jun. 2008.

[9] Z. Xing, K. Liu, and Y. Liu, "Closed-form and analytical BER expression for OFDM system with μ-law companding operation," *China Commun.*, vol. 16, no. 7, pp. 61–69, Jul. 2019.

[10] S. P. DelMarco, "General closed-form family of companders for PAPR reduction in OFDM signals using amplitude distribution modification," *IEEE Trans. Broadcast.*, vol. 60, no. 1, pp. 102–109, Mar. 2014.

[11] K. S. Ramtej and S. Anuradha, "New error function companding technique to minimize PAPR in LTE uplink communications," in *Proc. 23rd Nat. Conf. Commun. (NCC)*, Mar. 2017, pp. 1–5.

[12] N. Sharan, S. K. Ghorai, and A. Kumar, "Peak-to-average power ratio (PAPR) reduction using combination of precoding and companding techniques for VLC OFDM systems," in *Proc. TEQIP III Sponsored Int. Conf. Microw. Integr. Circuits, Photon. Wireless Netw. (IMICPW)*, May 2019, pp. 149–153.

[13] Z. Xing, K. Liu, and Y. Liu, "Low-complexity companding function design for PAPR reduction in OFDM systems," *IET Commun.*, vol. 14, no. 10, pp. 1581–1587, Jun. 2020.

[14] M. S. Ahmed, S. Boussakta, A. Al-Dweik, B. Sharif, and C. C. Tsimenidis, "Efficient design of selective mapping and partial transmit sequence using T-OFDM," *IEEE Trans. Veh. Technol.*, vol. 69, no. 3, pp. 2636–2648, Mar. 2020.

[15] T. Deepa and R. Kumar, "Performance analysis of μ-law companding & SQRT techniques for M-QAM OFDM systems," in *Proc. IEEE Int. Conf. Emerg. Trends Comput., Commun. Nanotechnol. (ICECCN)*, Mar. 2013, pp. 303–307.

[16] M. R. Hossain and K. T. Ahmmed, "Efficient PAPR reduction in DCT-SCFDMA system based on absolute exponential companding technique with pulse shaping," *Wireless Pers. Commun.*, vol. 97, no. 3, pp. 3449–3463, Dec. 2017.

[17] Y. G. Li and G. L. Stuber, *Orthogonal Frequency Division Multiplexing for Wireless Communications.* New York, NY, USA: Springer, 2006.

[18] H.-G. Ryu, T. Phuong Hoa, K. Mi Lee, S.-W. Kim, and J.-S. Park, "Improvement of power efficiency of HPA by the PAPR reduction and predistortion," *IEEE Trans. Consum. Electron.*, vol. 50, no. 1, pp. 119–124, Feb. 2004.

[19] E. Costa, M. Midrio, and S. Pupolin, "Impact of amplifier nonlinearities on OFDM transmission system performance," *IEEE Commun. Lett.*, vol. 3, no. 2, pp. 37–39, Feb. 1999.

[20] A. McAndrew, "An introduction to digital image processing with MAT-LAB notes for SCM2511 image processing," School Comput. Sci. Math., Victoria Univ. Technol., Melbourne, VIC, Australia, Tech. Rep. 1, vol. 264, 2004.

[21] R. C. Gonzalez, R. E. Woods, and S. L. Eddins, *Digital Image Processing Using MATLAB*, vol. 624. Upper Saddle River, NJ, USA: Pearson-Prentice-Hall, 2004.

[22] E. Al-Dalakta, A. Al-Dweik, A. Hazmi, C. Tsimenidis, and B. Sharif, "PAPR reduction scheme using maximum cross correlation," *IEEE Commun. Lett.*, vol. 16, no. 12, pp. 2032–2035, Dec. 2012.

[23] Y. Wang, D. A. Basnayaka, X. Wu, and H. Haas, "Optimization of load balancing in hybrid LiFi/RF networks," *IEEE Trans. Commun.*, vol. 65, no. 4, pp. 1708–1720, Apr. 2017.

[24] M. Tariq, A. Al-Dweik, B. Mohammad, H. Saleh, and T. Stouraitis, "Computational power evaluation for energy-constrained wireless communications systems," *IEEE Open J. Commun. Soc.*, vol. 1, pp. 308–319, 2020.

[25] M. Pätzold, M. Patzold, and M. Paetzold, *Mobile Fading Channels*, vol. 14. Hoboken, NJ, USA: Wiley, 2002.

ABDULWAHID MOHAMMED received the B.S. degree in communication engineering from Saad Dahlab University, Algeria, in 2010, and the M.S. degree in electronics and communication engineering from Cairo University, Egypt, in 2019. He is currently pursuing the Ph.D. degree in electronics and communication engineering from Al-Azhar University, Egypt. His research interests include NB-IoT, wireless communication systems, 5G/6G communication networks, artificial intelligence, and machine learning/deep learning.

AMIN NASSAR is currently a Professor with the Department of Electronics and Electrical Communications, Faculty of Engineering, Cairo University.

TAWFIK ISMAIL (Senior Member, IEEE) was a Postdoctoral Researcher in optical and wireless communications with the Technical Institute of Microwave and Photonic Engineering, University of Graz, Austria, in 2015. He joined the Optical Wireless Communication Research Group, Department of Engineering and Sciences, University of Oxford, U.K., in 2018, where he was involved in research of quantum communication in free space. He is currently the Director of the Wireless Intelligent Networks Research Center, Nile University. He is also an Associate Professor with the National Institute of Laser Enhanced Sciences, Cairo University, Egypt. He has established and leading a research group for optical and wireless communications at Cairo University, Egypt. He has held research stays with the Technical Institute of Microwave and Photonic Engineering, University of Graz, Austria, the American University of Cairo, Egypt, Cairo University, and the Malaviya National Institute of Technology, India. Since 2014, he has been jointly involved in several research projects funded nationally by NTRA, ASRT, STDF, and ITIDA, Egypt, and internationally by InnoveUK, U.K. His research interests include in the broad areas including optical and wireless communications, mmWave, mobile edge computing, cryptography, quantum communications, the IoT security, and blockchain, as well as the applications of artificial intelligence and machine learning in communication networks and healthcare.

HASSAN MOSTAFA (Senior Member, IEEE) received the B.Sc. and M.Sc. degrees (Hons.) in electronics engineering from Cairo University, Cairo, Egypt, in 2001 and 2005, respectively, and the Ph.D. degree in electrical and computer engineering from the Department of Electrical and Computer Engineering, University of Waterloo, Waterloo, ON, Canada, in 2011. He is currently an Associate Professor with the Nanotechnology and Nanoelectronics Program, Zewail City of Science and Technology, Giza, Egypt, on leave from the Department of Electronics and Electrical Communications, Cairo University. He was an NSERC Postdoctoral Fellow with the Department of Electrical and Computer Engineering, University of Toronto, Toronto, ON, Canada. He was a Postdoctoral Researcher in collaboration with Fujitsu Research Laboratories in Japan and USA with a focus on the design of the next-generation FPGA. He has authored/coauthored more than 170 articles in international journals and conferences and five published books. His research interests include neuromorphic computing, the IoT hardware security, software-defined radio, reconfigurable low-power systems, analog-to-digital converters, low-power circuits, subthreshold logic, variation-tolerant design, soft error-tolerant design, statistical design methodologies, next-generation FPGA, spintronics, memristors, energy harvesting, MEMS/NEMS, powermanagement, and optoelectronics. He has been a member of the IEEE Technical Committee of VLSI Systems and Applications since 2017. He was a recipient of the University of Waterloo SandFord Fleming TAExcellence Award in 2008, the Ontario Graduate Scholarship in 2009, the Waterloo Institute of Nano-Technology Nanofellowship Research Excellence Award in 2010, the Natural Sciences and Engineering Research Council of Canada Prestigious Postdoctoral Fellowship in 2011, and the University of Toronto Research Associate Scholarship in 2012.

● ● ●